Transient Simulation of Arbitrary Nonuniform Interconnection Structures Characterized by Scattering Parameters

Tom Dhaene, Luc Martens, and Daniël De Zutter

Abstract—**In this paper we present a new noniterative time-dependent circuit model for transient analysis of general uniform and nonuniform interconnection structures terminated with arbitrary linear or nonlinear loads. Simulated or measured scattering parameter data are used to characterize the interconnection structures. No approximations or model fitting are required. At each point in time, all coupled ports of the interconnection structure are modeled as extended Thevenin equivalents, which consist of constant resistances and time-dependent voltage sources. This new general circuit representation is compatible with existing simulation programs such as SPICE. Simulations on circuits with linear and nonlinear loads illustrate our approach.**

I. Introduction

NONUNIFORM interconnection structures are quite often used in microwave systems and in high-speed electronics. In chip carriers for example, the interconnections are usually nonuniform because of the high circuit density, the complex geometry, and the geometrical constraints at the edges of the chip. Nonuniform transmission lines are also used as filters, as couplers, as impedance matching sections, as equalizers, as resonators and as pulse transformers [1]–[8]. Some nonuniform transmission lines show good transmission responses and they are used to realize specific time-domain waveforms in various measurement systems [9], [10].

The study of transient propagation phenomena on general interconnection structures is very important for the synthesis and the design of high-speed electronic circuits. Transient analysis of general uniform transmission line structures has been extensively studied in the past [11]–[13]. However, the transient analysis of nonuniform interconnection structures is described by fewer authors.

Originally, these studies were restricted to particular nonuniform transmission lines such as binomial form coupled lines, and exponential or hyperbolic tapered lines [14]–[20]. In some specific cases closed-form solutions for the transient response have been found. Sometimes, the nonuniform structures have been simulated as a cascade of lumped elements and ideal lossless transmission lines. Such simple models can easily be implemented in existing circuit simulators.

Recently, the transient analysis of nonuniform lines has been addressed in much more detail. Yang, Kong, and Gu [21], [22] used a time-domain perturbational technique for the analysis of a pair of lossless nonuniform coupled transmission lines. This approach is based on many simplifying assumptions and is restricted to a limited class of lines. Palusinski and Lee [23] presented a new method based on a spectral method (with Chebyshev polynomials as interpolants). This complicated method is also restricted to frequency-independent structures, and its accuracy is limited. Orhanovic and Tripathi [24] proposed a transient simulation technique based on the generalized method of characteristics. The nonuniform transmission lines are discretized along their length, which increases the simulation time and the memory requirements. Mehalic and Mittra [25] studied the transient responses on tapered multiple microstrip lines. The interconnection structures are characterized by modal scattering parameters and the modal decoupling is supposed to be frequency-independent. Winklestein, Steer and Pomerleau [26], [27] presented an iterative simulation algorithm for uniform and nonuniform transmission lines. In fact, the interconnection lines are modeled by a number of time-dependent nonlinear voltage sources. More recently, Chang [28] proposed an iterative simulation algorithm for single nonuniform dispersive transmission lines, based on the waveform relaxation method. Gu, Sheen, and Ali [29] presented a new rather complicated iterative (time-consuming) method that describes the nonuniform structures by a set of nonlinear algebraic equations. Mao and Li [30], [31] proposed two new methods. The first one [30] uses a new method of convolution characteristics, and the second one [31] models the nonuniform transmission lines by a cascaded chain of many multiport subnetworks which are made of short sections of uniform lines. Both methods are restricted to some particular nonuniform structures. The method presented by Schutt-Aine [32] is limited

Manuscript received April 1, 1992; revised September 9, 1992. This work was supported by a grant to T. Dhaene from IWONL. This paper was recommended by W. W.-M. Dai.

The authors are with the Laboratory of Electromagnetism and Acoustics, University of Ghent, 9000 Ghent, Belgium.

IEEE Log Number 9205571.

to special single lossless nonuniform transmission line structures. In [30]–[32], the nonuniform transmission lines must be discretized along their length, which increases the number of nodes in the network, the computation time, and the memory requirements dramatically.

In this paper we present a new elegant noniterative approach for transient analysis of very general interconnection structures characterized by (simulated or measured) scattering parameters and terminated with arbitrary linear or nonlinear loads and sources. Generally speaking, the characteristics of the interconnection structures can be frequency-dependent. No approximations or model fitting is required. We use the time-domain scattering parameters to determine the interaction of the interconnections with the arbitrary loads.

Scattering parameters [33] are well suited for the characterization and the modeling of linear high-frequency devices. Some circuit simulators and some electromagnetic simulation programs [34] can calculate S-parameters very accurately. Scattering parameters are easier to measure and to work with at high frequencies than other types of parameters. They are numerically well defined. Using careful calibration techniques, high quality measurements can be performed. Scattering parameters are conceptually simple. They can be interpreted as the energy which is reflected by or transmitted through a linear structure. They relate to familiar concepts such as gain, loss and reflection coefficient. S-parameters can provide a surprising degree of insight into a measurement or design problem. However, many digital designers in telecommunication and computer applications feel more comfortable with time-domain data than with frequency-domain data, and they prefer transient simulation results.

In this paper, the transient simulation problem is handled in a time-stepping way. At each point in time, all coupled ports of the high-speed interconnection structure under study are modeled as simple equivalent Thevenin (or Norton) networks. So, the simulation problem can be solved with traditional circuit techniques. This new algorithm of general validity can be seen as a generalization and an extension of the simulation method for uniform and nonuniform lines presented in [13] and [35]. The frequency dependence of the coupling between different ports of the interconnection structure is explicitly taken into account. The algorithm can also be used to calculate eye-diagrams or to transform S-parameters data into time domain reflection (TDR) or time-domain transmission (TDT) pictures [36]. The advantage of this method over the other techniques resides in its flexibility, its computational stability, its noniterative character, its simple Thevenin representation and its compatibility with existing circuit simulators such as SPICE. We illustrate this new general approach by several examples with linear and nonlinear loads.

II. Frequency-Domain Description

In this section, we construct an extended equivalent Thevenin circuit model in the frequency domain for general high-speed interconnection structures which are characterized in terms of scattering parameters.

We consider a general linear stationary active or passive interconnection structure with a total of N ports. For a high-speed or high-frequency interconnection structure one typically thinks of these ports as lines (e.g., microstrip or striplines, or perhaps even slotlines) carrying a certain signal in the form of a mode propagating along that line. We now explicitly want to allow one or more sets of coupled lines. We therefore group the N original single ports into M sets of coupled ports. Each coupled port p ($p = 1,\cdots, M$) consists of N_p of the original (uncoupled) ports. This means that:

$$N = \sum_{p=1}^{M} N_p \geq M. \tag{1}$$

N_p fundamental modes can propagate at the reference plane of the pth coupled port. Inside the interconnection structure higher-order modes may locally be activated. In Fig. 1, the general interconnection structure under study is shown.

The above division in a set of M coupled ports can also be understood as follows. Suppose a signal is presented at (uncoupled) port 1 of Fig. 1. Because this port is a part of the coupled port 1, i.e., of a set of N_1 coupled lines, a signal can immediately appear at ports 2 to N_1 of coupled port 1. The other ports of the structure are not part of coupled port 1. Hence the signal launched at port 1 will only reach these remaining ports after a certain delay time dictated by the nature of the structure under study.

For example, a set of T coupled uniform or nonuniform transmission lines has $2T$ (uncoupled) ports. Both sides of the transmission line structure will be seen as a coupled port consisting of T (uncoupled) ports.

We assume that the (traditional) S-parameters of the general interconnection structure are known on a single port basis from measurements or from simulations. The reference resistance associated with port n ($n = 1,\cdots, N$) is represented by R_n. Quite often this reference impedance is 50 Ω. We use a vector notation to compactly represent all relevant variables. $\boldsymbol{A_p}$ ($= [A_{p_i}]_{[N_p \times 1]}$) and $\boldsymbol{B_p}$ ($= [B_{p_i}]_{[N_p \times 1]}$) are the incident and reflected voltage wave vectors at the coupled port p ($p = 1,\cdots, M$), and $\boldsymbol{V_p}$ ($= V_{p_i}]_{[N_p \times 1]}$) and $\boldsymbol{I_p}$ ($= [I_{p_i}]_{[N_p \times 1]}$) are the associated voltage and current vectors, respectively. The above vectors are matrices with N_p rows and only a single column, i.e., i runs from 1 to N_p. We represent the coupled reference impedance matrix associated with the coupled port p by $\boldsymbol{R_p}$ ($= \text{diag}(R_{p_i})_{[N_p \times N_p]}$). This is a real, frequency-independent and diagonal matrix with elements R_{p_i}.

The frequency-domain voltage vector $\boldsymbol{V_p}(\omega)$ is the sum of the incident and the reflected voltage wave vectors at port p:

$$\boldsymbol{V_p}(\omega) = \boldsymbol{A_p}(\omega) + \boldsymbol{B_p}(\omega) \tag{2}$$

while the frequency domain current $\boldsymbol{I_p}(\omega)$ is the difference of the incident and the reflected voltage wave vec-

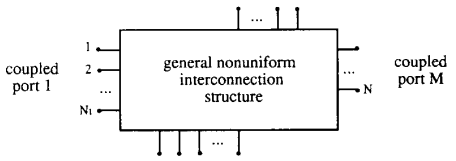

Fig. 1. General nonuniform interconnection structure.

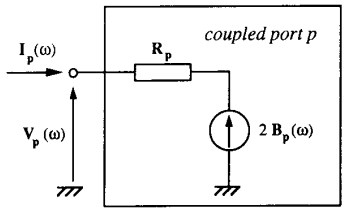

Fig. 2. Extended (frequency-domain) Thevenin model of coupled port p.

tors at port p divided by the local reference impedance matrix:

$$\boldsymbol{I}_p(\omega) = \boldsymbol{R}_{p'}^{-1}\left[\boldsymbol{A}_p(\omega) - \boldsymbol{B}_p(\omega)\right]. \tag{3}$$

The reference direction of $\boldsymbol{I}_p(\omega)$ is pointed towards the pth coupled port of the interconnection structure.

The relations between the traveling voltage wave vectors $\boldsymbol{A}(\omega)$ and $\boldsymbol{B}(\omega)$ of the whole interconnection structure are described in an unambiguous way by the overall scattering matrix $\boldsymbol{S}(\omega)$ and by the internal source vector $\boldsymbol{C}(\omega)$ [37]:

$$\boldsymbol{B}(\omega) = \boldsymbol{S}(\omega)\boldsymbol{A}(\omega) + \boldsymbol{C}(\omega). \tag{4}$$

Rewriting $\boldsymbol{A}(\omega)$ and $\boldsymbol{B}(\omega)$ in terms of $\boldsymbol{A}_p(\omega)$ and $\boldsymbol{B}_p(\omega)$ defined above allows us to recast (4) into the following form:

$$\begin{pmatrix} \boldsymbol{B}_1(\omega) \\ \cdots \\ \boldsymbol{B}_M(\omega) \end{pmatrix} = \begin{pmatrix} \boldsymbol{S}_{11}(\omega) & \cdots & \boldsymbol{S}_{1M}(\omega) \\ \cdots & & \\ \boldsymbol{S}_{M1}(\omega) & & \boldsymbol{S}_{MM}(\omega) \end{pmatrix} \cdot \begin{pmatrix} \boldsymbol{A}_1(\omega) \\ \cdots \\ \boldsymbol{A}_M(\omega) \end{pmatrix} + \begin{pmatrix} \boldsymbol{C}_1(\omega) \\ \cdots \\ \boldsymbol{C}_M(\omega) \end{pmatrix}. \tag{5}$$

$\boldsymbol{C}_p(\omega)$ $(p = 1,\cdots, M)$ now represents the impressed voltage wave vector on a per coupled port basis. $\boldsymbol{S}_{pp}(\omega)$ $(p = 1,\cdots, M)$ can be seen as a scattering reflection coefficient matrix, while $\boldsymbol{S}_{pq}(\omega)$ $(p \neq q$ and $p, q = 1,\cdots, M)$ can be seen as a scattering transmission coefficient matrix.

Combining (2), (3), (4), and (5) gives the following matrix relations:

$$\begin{aligned} \boldsymbol{V}_p(\omega) &= \boldsymbol{R}_p\boldsymbol{I}_p(\omega) + 2\boldsymbol{B}_p(\omega) \\ &= \boldsymbol{R}_p\boldsymbol{I}_p(\omega) + 2\sum_{q=1}^{M} \boldsymbol{S}_{pq}(\omega)\boldsymbol{A}_q(\omega) + 2\boldsymbol{C}_p \end{aligned} \tag{6}$$

$$\boldsymbol{A}_p(\omega) = 0.5\left[\boldsymbol{V}_p(\omega) + \boldsymbol{R}_p\boldsymbol{I}_p(\omega)\right]. \tag{7}$$

Equation (6) learns that the voltage $\boldsymbol{V}_p(\omega)$ at the coupled port p is related with the current $\boldsymbol{I}_p(\omega)$ and the reflected voltage waves $\boldsymbol{B}_p(\omega)$ at the same coupled port. In Fig. 2, the coupled port p is represented as an extended equivalent Thevenin circuit (in the frequency domain).

III. Time-Domain Description

In this section, we construct an extended time-dependent equivalent Thevenin model for a general N-port interconnection structure by transforming the frequency-domain description to the time domain. All multiplications in the frequency domain transform to convolutions in the time domain.

Inverse Fourier transformation of (6) and (7) gives, respectively,

$$\begin{aligned} \boldsymbol{v}_p(t) &= \boldsymbol{R}_p\boldsymbol{i}_p(t) + 2\boldsymbol{b}_p(t) \\ &= \boldsymbol{R}_p\boldsymbol{i}_p(t) + 2\sum_{q=1}^{M} \boldsymbol{s}_{pq}(t) * \boldsymbol{a}_q(t) + 2\boldsymbol{c}_p(t) \end{aligned} \tag{8}$$

$$\boldsymbol{a}_p(t) = 0.5\left[\boldsymbol{v}_p(t) + \boldsymbol{R}_p\boldsymbol{i}_p(t)\right] \tag{9}$$

where $*$ represents the convolution operator, where $\boldsymbol{b}_p(t)$ and $\boldsymbol{a}_p(t)$ are the time-domain traveling voltage wave vectors, where $\boldsymbol{c}_p(t)$ is the time-domain impressed voltage wave vector, where $\boldsymbol{v}_p(t)$ and $\boldsymbol{i}_p(t)$ represent the time-domain voltage and current vectors, respectively, and where $\boldsymbol{s}_{pq}(t)$ $p, q = 1,\cdots, M)$ are impulse response matrices (time domain Green's functions) as will be proved in Section IV.

Due to the specific way in which we grouped the ports (see the discussion immediately after (1)), we can state that

$$\boldsymbol{s}_{pq}(t = 0) = 0 \qquad p \neq q \quad \text{and} \quad p, q = 1,\cdots, M. \tag{10}$$

Otherwise, we would have regarded the coupled ports p and q as one single coupled port. Physically, this means that it takes some time to transmit a signal from coupled port q to coupled port p $(p \neq q)$. Equation (10) corresponds with

$$\lim_{\omega\to\infty}\left\{\boldsymbol{S}_{pq}(\omega)\right\} = 0 \qquad p \neq q \quad \text{and} \quad p, q = 1,\cdots, M \tag{11}$$

in the frequency domain.

On the other hand, $\boldsymbol{s}_{pp}(t = 0)$, will not be equal to zero in the general case. We split the (frequency domain) matrix $\boldsymbol{S}_{pp}(\omega)$ $(p = 1,\cdots, M)$ in a frequency-independent term $\boldsymbol{S}_{pp}^{\lim,im}$ and a frequency-dependent term $\tilde{\boldsymbol{S}}_{pp}(\omega)$:

$$\boldsymbol{S}_{pp}(\omega) = \boldsymbol{S}_{pp}^{\lim} + \tilde{\boldsymbol{S}}_{pp}(\omega) \qquad p = 1,\cdots, M \tag{12}$$

where

$$\lim_{\omega\to\infty}\left\{\boldsymbol{S}_{pp}(\omega)\right\} = \boldsymbol{S}_{pp}^{\lim}, \qquad p = 1,\cdots, M. \tag{13}$$

$S_{pp}^{\lim}$, is the instantaneous ($t = 0$) reflection coefficient seen at the coupled port p. This constant part $S_{pp}^{\lim}$ can be transformed in an analytical way while the frequency-dependent part $\tilde{S}_{pp}(\omega)$ can be transformed numerically. So, (12) transforms to

$$s_{pp}(t) = S_{pp}^{\lim}\,\delta(t) + \tilde{s}_{pp}(t) \qquad p = 1,\cdots,M \quad (14)$$

in the time domain. The behavior of $s_{pp}(t)$ at $t = 0$ is dominated by the factor $S_{pp}^{\lim}\,\delta(t)$. One can prove that $\tilde{s}_{pp}(t)$ ($p = 1,\cdots,M$) is regular in the time-interval $[0\text{–}0^+]$ for all physical possible reflection coefficients $S_{pp}(\omega)$ (finite energy). This ensures that

$$\int_0^{0+} \tilde{s}_{pp}(\tau)\boldsymbol{a}_p(t-\tau)\,d\tau = 0 \qquad p = 1,\cdots,M. \quad (15)$$

If we introduce (14) in (8) and take into account (10), (15), and the fact that $\tilde{s}_{pp}(t) = s_{pp}(t)$ for $t \geq 0^+$, then (8) is reformulated as

$$\boldsymbol{v}_p(t) = \boldsymbol{R}_p\boldsymbol{i}_p(t) + 2S_{pp}^{\lim}\,\boldsymbol{a}_p(t) + 2\boldsymbol{c}_p(t) + 2\sum_{q=1}^{M}\int_{0+}^{t} s_{pq}(\tau)\boldsymbol{a}_q(t-\tau)\,d\tau. \quad (16)$$

The first three terms of (16) depend only on the instantaneous reaction of the structure at time t, while the fourth term contains all other factors. Taking (9) into account, (16) reduces to

$$\boldsymbol{v}_p(t) = \left[\mathbf{1} - S_{pp}^{\lim}\right]^{-1}\left\{\left[\mathbf{1} + S_{pp}^{\lim}\right]\boldsymbol{R}_p\boldsymbol{i}_p(t) + 2\sum_{q=1}^{M}\int_{0+}^{t} s_{pq}(\tau)\boldsymbol{a}_q(t-\tau)\,d\tau + 2\boldsymbol{c}_p(t)\right\} \quad (17)$$

or

$$\boldsymbol{v}_p(t) = \boldsymbol{R}'_p\boldsymbol{i}_p(t) + 2\sum_{q=1}^{M}\int_{0+}^{t} s'_{pq}(\tau)\boldsymbol{a}_q(t-\tau)\,d\tau + 2\boldsymbol{c}'_p(t) \quad (18)$$

where

$$\boldsymbol{R}'_p = \left[\mathbf{1} - S_{pp}^{\lim}\right]^{-1}\left[\mathbf{1} + S_{pp}^{\lim}\right]\boldsymbol{R}_p \quad (19)$$

$$s'_{pq}(t) = \left[\mathbf{1} - S_{pp}^{\lim}\right]^{-1} s_{pq}(t) \quad (20)$$

$$\boldsymbol{c}'_p(t) = \left[\mathbf{1} - S_{pp}^{\lim}\right]^{-1}\boldsymbol{c}_p(t). \quad (21)$$

The impedance matrix $\boldsymbol{R}'_p$, is equal to the local instantaneous characteristic impedance matrix seen at port p ($p = 1,\cdots,M$), and this matrix will be nondiagonal in the general case. Note that $\boldsymbol{R}'_p = \boldsymbol{R}_p$, $s'_{p,q}(t) = s_{pq}(t)$ and $\boldsymbol{c}'_p(t) = \boldsymbol{c}_p(t)$ if $s_{pp}^{\lim}(0) = 0$.

The transient simulation problem is handled in a time-stepping fashion. All equations are discretized before computer implementation. So, (9) and (16) respectively reduce to:

$$\boldsymbol{a}_p(g-h) = 0.5\left[\boldsymbol{v}_p(g-h) + \boldsymbol{R}_p\boldsymbol{i}_p(g-h)\right] \quad (22)$$

and

$$\boldsymbol{v}_p(g) = \boldsymbol{R}_p\boldsymbol{i}_p(g) + 2\left[S_{pp}^{\lim} + \tilde{s}_{pp}(0)\Delta t\right]\boldsymbol{a}_p(g) + 2\sum_{q=1}^{M}\sum_{h=1}^{g} s_{pq}(h)\boldsymbol{a}_q(g-h)\Delta t + 2\boldsymbol{c}_p(g) \quad (23)$$

where Δt is the time step, and g and h stand for the discretized times $g\Delta t$ and $h\Delta t$. The first factor $(2\tilde{s}_{pp}(0)\Delta t\boldsymbol{a}_p(g))$ of the summation which depends on the instantaneous time $g\Delta t$ is explicitly written. We reformulate (23) as

$$\boldsymbol{v}_p(g) = \boldsymbol{R}'_p\boldsymbol{i}_p(g) + 2\sum_{q=1}^{M}\sum_{h=1}^{g} s'_{pq}(h)\boldsymbol{a}_q(g-h)\Delta t + 2\boldsymbol{c}'_p(g) = \boldsymbol{R}'_p\boldsymbol{i}_p(g) + 2\boldsymbol{b}'_p(g) \quad (24)$$

where now

$$\boldsymbol{R}'_p = \left[\mathbf{1} - S_{pp}^{\lim} - \tilde{s}_{pp}(0)\Delta t\right]^{-1}\cdot\left[\mathbf{1} + S_{pp}^{\lim} + \tilde{s}_{pp}(0)\Delta t\right]\boldsymbol{R}_p \quad (25)$$

$$s'_{pq}(g) = \left[\mathbf{1} - S_{pp}^{\lim} - \tilde{s}_{pp}(0)\Delta t\right]^{-1} s_{pq}(g) \quad (26)$$

$$\boldsymbol{c}'_p(g) = \left[\mathbf{1} - S_{pp}^{\lim} - \tilde{s}_{pp}(0)\Delta t\right]^{-1}\boldsymbol{c}_p(g). \quad (27)$$

$\boldsymbol{b}'_p(g)$ can be considered as a voltage source vector that depends on previous voltages waves.

Consequently, at each point in time, all coupled ports of a general high-speed interconnection structure can be represented by an equivalent circuit model. In Fig. 3, an extended time-domain Thevenin model for the coupled port p is shown. Of course, this can also be represented by an extended time domain Norton model.

IV. Physical Interpretation and Implementation of the Method

The calculation of the inverse Fourier transform is the most difficult numerical procedure involved in the formulation of the transient simulation algorithm. Sometimes $S_{pq}(\omega)$ ($p, q = 1,\cdots,M$) goes to a periodic function as ω approaches infinity and $S_{pp}^{\lim}$ cannot be determined analytically. In that case we use the inverse fast Fourier transform (FFT) and a bandlimiting window to determine $s_{pq}(t)$. Before transforming the scattering parameters to the time domain, the frequency-domain data are bandlimited in order to avoid ringing and aliasing errors. Normally, we use a Hamming window as low-pass filter [38]. The windowing results in a minor spreading of the final results (some additional loss and dispersion in the simulated transient response) [26].

The time-domain S-parameters $s_{pq_{ij}}(t)$ ($p, q = 1,\cdots,M$; $i = 1,\cdots,N_p$; $j = 1,\cdots,N_q$) can be interpreted physically. Suppose that $\boldsymbol{c}_p(t) = 0$ (no internal sources) and that each coupled port p ($p = 1,\cdots,M$) of the interconnection

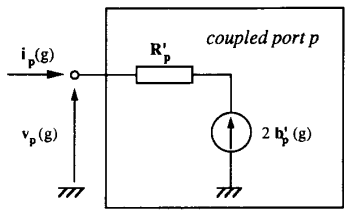

Fig. 3. Extended (time-domain) Thevenin equivalent of coupled port p at time $g\Delta t$.

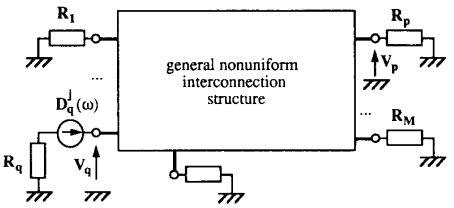

Fig. 4. General interconnection structure excited by a voltage impulse.

structure under study is terminated by its reference impedance matrix $\boldsymbol{R}_p$. This network configuration is shown in Fig. 4. A voltage source of amplitude 1 is applied at port j of coupled port q. $\boldsymbol{D}^j_q(\omega)$ $(= [D^j_{q,k}(\omega)]_{[N_q \times 1]})$ is a voltage source vector where $D^j_{q,j}(\omega) = 1$ and $D^j_{q,k}(\omega) = 0$ if $k \neq j$. Combining (2), (3), and (4) gives

$$V_{p_i}(\omega) = 0.5\, S_{pq_{ij}}(\omega) \tag{28}$$

Hence, the transfer function $S_{pq_{ij}}(\omega)$, which is an element of $\boldsymbol{S}_{pq}(\omega)$, is the resulting voltage at port i of coupled port p if a voltage source of amplitude 1 (for all frequencies) is applied at port j of coupled port q. In the time domain, (28) corresponds with:

$$v_{p_i}(t) = 0.5\, s_{pq_{ij}}(t). \tag{29}$$

$s_{pq_{ij}}(t)$ is equal to twice the voltage at port i of coupled port p if a voltage impulse $\delta(t)$ is applied at port j of coupled port q at $t = 0$. Thus $s_{pq_{ij}}(t)$ $(p, q = 1, \cdots, M;$ $i = 1, \cdots, N_p;$ $j = 1, \cdots, N_q)$ can be interpreted as impulse responses.

Once the local instantaneous characteristic impedance matrices $\boldsymbol{R}'_p$, (19) are known $(p = 1, \cdots, M)$, these matrices can be used as reference matrices and the extended scattering matrices (ESM) can be calculated. The overall scattering parameter matrix $\boldsymbol{S}(\omega)$ (corresponding with the diagonal reference matrices $\boldsymbol{R}_p$) can be transformed to the extended scattering parameter matrix $\boldsymbol{S}^{\mathrm{ESM}}(\omega)$ (corresponding with the nondiagonal reference matrices $\boldsymbol{R}'_p$):

$$\boldsymbol{S}^{\mathrm{ESM}}(\omega) = [(\boldsymbol{T} + \boldsymbol{1}) + \boldsymbol{S}(\omega)(\boldsymbol{T} - \boldsymbol{1})]^{-1}[(\boldsymbol{T} - \boldsymbol{1}) + \boldsymbol{S}(\omega)(\boldsymbol{T} + \boldsymbol{1})] \tag{30}$$

where

$$\boldsymbol{T} = \boldsymbol{R}\boldsymbol{R}'^{-1} = [\boldsymbol{R}_p]_{[M \times M]}[\boldsymbol{R}_p{}']^{-1}_{[M \times M]}. \tag{31}$$

Using these extended scattering parameters, the transient analysis proceeds in a completely analogous way as described earlier. However, thanks to the particular choice of the reference matrices the (time-domain) impulse functions $\boldsymbol{s}^{\mathrm{ESM}}(t)$ will have a relatively short time-duration, and $\boldsymbol{s}^{\mathrm{ESM}}(0) = 0$. Short impulse responses are important for the stability and accuracy of the simulation method. They facilitate the inverse transformation problem, increase the computational speed of the algorithm and decrease the memory requirements and the cumulated errors.

The simulation algorithm is outlined in Fig. 5. First, the nonuniform general dispersive interconnection structure under study is characterized in the frequency domain by its (measured or simulated) scattering matrix. If necessary, each coupled port of the interconnection structure can have a different reference impedance matrix. These reference matrices can be chosen to be equal to the local instantaneous characteristic impedance matrices of the coupled ports. Next, we use the FFT-algorithm to transform the frequency-domain data into impulse responses. These impulse functions can have a relatively short duration thanks to the particular choice of the reference matrices. Finally, the transient problem is solved in a time-marching way: after each step in time, the relevant model parameters are computed by convolving the impulse responses with previous voltage waves. At each point in time, all coupled ports of the interconnection structure are reduced to an extended Thevenin circuit model, and the simulation problem is solved with traditional circuit techniques. The Thevenin circuit models are implemented in a new SPICE-like transient simulator (TMSIM). In this simulator, all time derivatives are numerically approximated by finite differences. The Modified Nodal Approach (MNA) is used to formulate the discretized circuit equations [39], and the Newton–Raphson algorithm is used to handle the nonlinear elements in the circuit. The elementary (MNA-) stamp corresponding to the interconnection structure is given by

$$\begin{pmatrix} \boldsymbol{1} & \boldsymbol{1} \\ \boldsymbol{1} & -\boldsymbol{R}'_p \end{pmatrix} \begin{pmatrix} \boldsymbol{v}_p(g) \\ \boldsymbol{i}_p(g) \end{pmatrix} = \begin{pmatrix} 2\boldsymbol{b}'_p(g) \end{pmatrix} \tag{32}$$

where $\boldsymbol{1}$ is an identity N_p by N_p matrix.

Owing to the time marching method used, very small errors can accumulate. So, as the total simulated time t increases, the size of the errors may slightly increase. Increasing the number of points involved in the calculation of the Green's functions decreases the errors.

V. Numerical Results

To illustrate the advantages and the possibilities of this new powerful SPICE-like simulator, we give some representative examples.

Example 1: Tapered Microstrip Line

We consider a tapered microstrip line. The top view and the cross section are shown in Fig. 6. The scattering parameters of this nonuniform interconnection structure

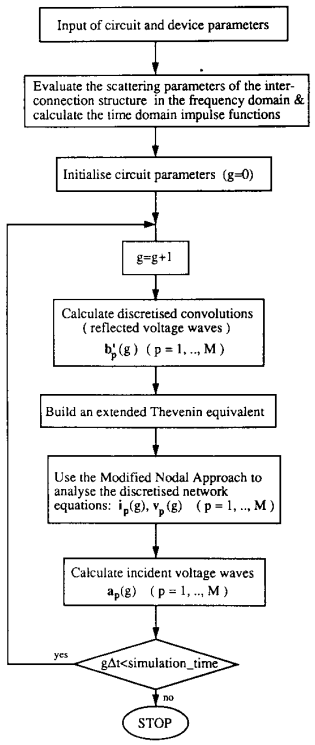

Fig. 5. Flow chart of simulation algorithm.

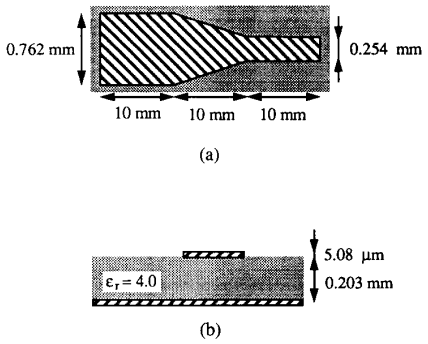

Fig. 6. Tapered microstrip line. (a) Top view. (b) Cross section.

were calculated with HP-MDS (Microwave Design System) [34]. The magnitude of S_{11} and S_{21} are shown in Fig. 7. The conductor is assumed to be lossless. Tapered lines are often used as impedance matching sections in high-speed chip-packages and multichip modules. The network configuration under study is shown in Fig. 8. The source generates an alternating on-off signal of 2 Gbit/s. The (10–90%) rise and fall time (80 ps) are 4/25 of the bitperiod (500 ps). This corresponds with a bandwidth of 6 GHz (99% coverage of the power spectrum). The voltage source has an internal impedance of 33.4 Ω. The tapered line is terminated with a 65.4-Ω resistor. This guarantees a perfect match at both sides. The simulation

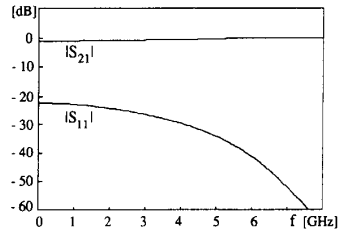

Fig. 7. $|S_{11}|$ and $|S_{21}|$ of tapered microstrip line.

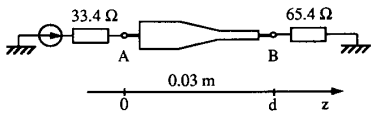

Fig. 8. Linear network configuration with tapered line.

time step is chosen to be 10 ps. Fig. 9 shows the voltages at the generator (A) and at the load (B). Remark the inductive effect of the taper: the current is forced to concentrate in a smaller area owing to the change of width that causes an inductive effect.

The results of this time-domain simulation method are in good agreement with frequency-domain methods [40]. It is important to note that a frequency-domain simulation algorithm calculates the steady-state response, while a time-domain simulation algorithm calculates the transient behavior!

Example 2: High-Speed High-Density Multichip Module Connector

Time-domain analysis of nonlinear networks is indispensable for system design. Based on accurate high-frequency measurements, we can simulate the transient behavior of complex three-dimensional interconnection structures.

The scattering parameters of a high-speed high-density multichip module (MCM) connector were measured in the frequency range 45 MHz–15 GHz with a new measurement set-up, using coplanar probe heads [41]. The surface mounted multichip module connector is "sandwiched" between a PCB mother board and a daughter board. A 3D-view is shown in Fig. 10. The contact points $A', C', E', \cdots$ on the daughter board are connected with respectively $B', D', F', \cdots$ on the mother board through the MCM-connector. The contacts A'–B' and C'–D' in the connector are separated from the other signal contacts (E'–$F', \cdots$) by ground contacts. Hence, we can neglect the interaction with the other contacts and it makes sense to consider A'–B'–C'–D' as a four port. From the measurements (obtained with a HP8510B vector network analyzer), it was derived that the connector has a good performance up to 3.5 GHz. In Fig. 11, the reflection at port B' ($|S_{11}|$) and the transmission from B' to A' ($|S_{21}|$) are shown.

We consider the nonlinear network configuration of Fig. 12. The internal impedance of the generator is 50 Ω.

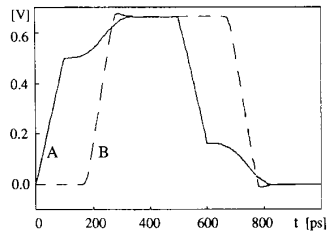

Fig. 9. Voltages at generator A (——) and at load B (– –) of tapered line.

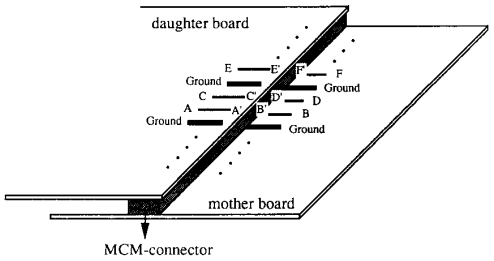

Fig. 10. 3-D view of multichip module connector.

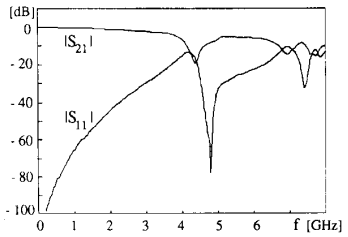

Fig. 11. $|S_{11}|$ and $|S_{21}|$ of MCM connector.

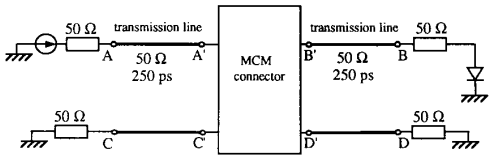

Fig. 12. Nonlinear network configuration with MCM connector.

The voltage source generates a pulse with an amplitude of 1 V and a width of 2 ns at its half amplitude (500 Mbit/s). The (10–90%) rise and fall time is 125 ps. Most ports of the interconnection structure are quasi-matched. At the right-hand side, the active line is terminated in a series combination of a 50-Ω resistor and a diode characterized by

$$i = I_A\left(\exp\left(\frac{v}{V_T}\right) - 1\right) \tag{33}$$

where $I_A = 20$ nA and $V_T = 30$ mV.

Fig. 13 shows the calculated responses. The full (dashed-) line shows the voltage at the left- (right-) hand side of the activated line. The reflections caused by the connector are rather small. The simulation time step was chosen to be 10 ps. We calculated 1000 steps in time. The CPU time used was 32 s on a DEC-3100 workstation.

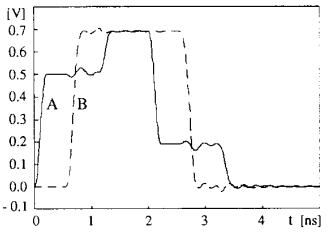

Fig. 13. Voltages at generator A (——) and at load B (– –) on activated line of Fig. 12.

Example 3: Uniform Coupled Dispersive Lossy Transmission Lines

The simulation tool developed in this paper can also be used for transient analysis of uniform coupled lossy dispersive lines. As an example, we consider an asymmetric two-line microstrip configuration supported by a lossy substrate (see Fig. 14). Using a new high-frequency circuit model [42] and a new rigorous full-wave integral equation technique [43], the frequency-dependent line parameter matrices are calculated in the frequency range 0 Hz–100 GHz (Fig. 15). The dielectric losses are important and are taken into account in an exact way. On the other hand, the resistive losses are neglected, i.e., the conductors are taken to be perfectly conducting ($\Rightarrow \boldsymbol{R}(\omega) \approx 0$). The full-wave line parameter matrices ($\boldsymbol{R}(\omega)$, $\boldsymbol{G}(\omega)$, $\boldsymbol{L}(\omega)$, and $\boldsymbol{C}(\omega)$) are used to calculate the extended scattering parameters of the four-port transmission structure.

The coupled transmission line network is shown in Fig. 16. The source generates a voltage pulse with an amplitude of 1 V and a width of 500 ps at its half amplitude (2 Gbit/s). The (10–90%) rise and fall time is 80 ps. The internal impedance of the generator is 40 Ω. The transmission line structure is quasi-matched at the generator side. At the load side, both lines are terminated in a series combination of a resistor and diode which is shunted by a capacitor C. The relation between the current i through and the voltage v over the diode is given by (33), where $I_A = 10$ nA and $V_T = 20$ mV.

The transient simulation results are represented in Fig. 17. The value of the capacitor C is varied over two decades: the capacitance is respectively 1 pF, 10 pF, and 100 pF in Fig. 17(a)–(b), (c)–(d), and (e)–(f). Fig. 17(a), (c), and (e) show the voltages on the activated line, while Fig. 17(b), (d), and (f) show the voltages on the passive line. The full (dashed-) lines show the voltage at the left- (right-) hand side of the transmission line structure, while the dotted lines show the voltage over the diodes.

If a large capacitor (100 pF) is placed in parallel with the diode, the diode is always in cut-off and the right-hand side of the transmission line is quasi-matched. This limits the reflections. If the capacitance decreases, the voltage

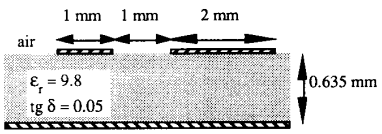

Fig. 14. Cross-section of asymmetric two-line microstrip configuration.

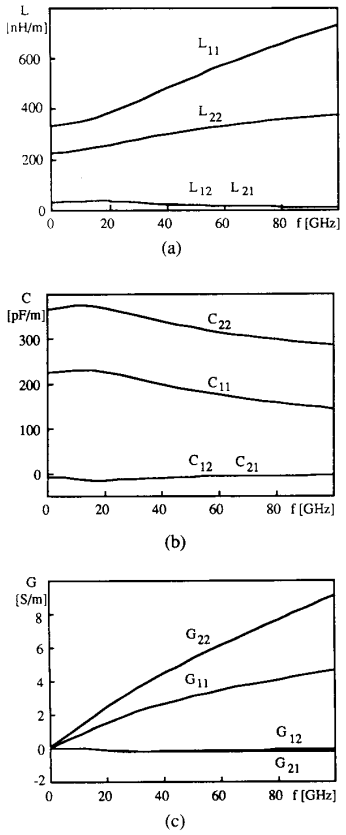

Fig. 15. Frequency-dependent transmission line parameter matrices. (a) Inductance matrix $\boldsymbol{L}(\omega)$. (b) Capacitance matrix $\boldsymbol{C}(\omega)$. (c) Conductance matrix $\boldsymbol{G}(\omega)$.

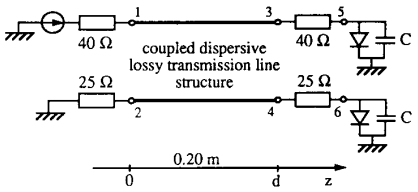

Fig. 16. Coupled dispersive transmission line network with nonlinear loads.

across the diode builds up much faster. Once the threshold voltage is reached, the diode starts conducting and changes from an open to a short circuit. The reflections are much higher in this case. Note that the transmitted signals are spread out owing to the dispersion.

The nonlinear elements were linearized with an iteration scheme based on the Newton–Raphson algorithm. The simulation time step was chosen to be 8 ps. We calculated 1000 steps in time. The CPU time used was 95 s on a DEC-3100 workstation.

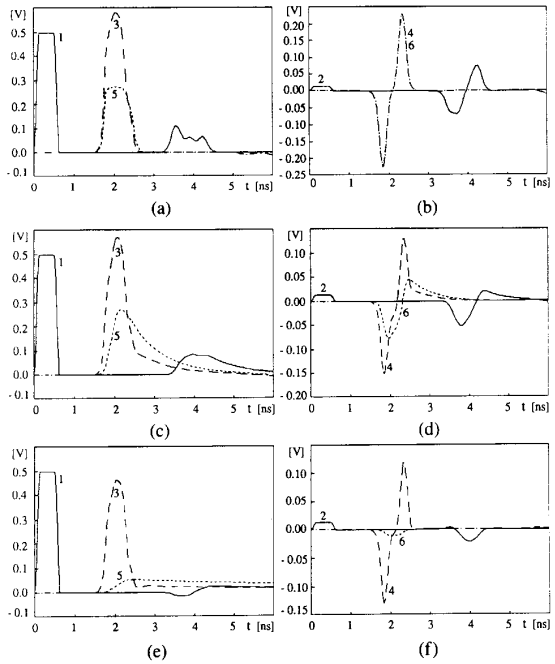

Fig. 17. Responses of the transmission line network of Fig. 16. (a), (c), (e): voltages on active line; (b), (d), (f): voltages on passive line; (a) and (b): $C = 1$ pF. (c) and (d) $C = 10$ pF. (e) and (f) $C = 100$ pF.

Example 4: Reference Example

Consider the coupled transmission line network shown in Fig. 18. This reference example was introduced by Djordjevic *et al.* [11], and was later used by Winklestein *et al.* [26], [27]. The active line is driven by a voltage source that generates a pulse of 6 ns with a rise and fall time of 1.5 ns. The left-hand side of the passive line is terminated in a 75-Ω resistor. At the right-hand side, both lines are terminated in a series combination of a 10-Ω resistor and a diode resistor. The relation between the current i through and the voltage v over the diode is given by (33) where $I_A = 10$ nA and $V_T = 25$ mV.

The transmission line parameter matrices are

$$\boldsymbol{R} = \begin{bmatrix} 524 & 33.9 \\ 33.9 & 524 \end{bmatrix} \sqrt{f}\,\mu\Omega/\text{m} \quad \boldsymbol{L} = \begin{bmatrix} 309 & 21.7 \\ 21.7 & 309 \end{bmatrix} \text{nH/m}$$

$$\boldsymbol{G} = \begin{bmatrix} 0.905 & -0.0118 \\ -0.0118 & 0.905 \end{bmatrix} f \text{ pS/m}$$

$$\boldsymbol{C} = \begin{bmatrix} 144 & -6.4 \\ -6.4 & 144 \end{bmatrix} \text{pF/m}. \tag{34}$$

The line-resistance matrix varies with the square root of the frequency f, due to the skin-effect losses, whereas the line-conductance matrix varies proportionally with the frequency.

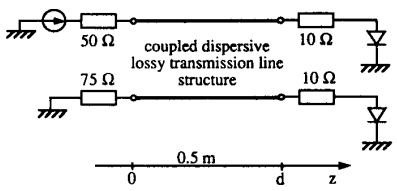

Fig. 18. Coupled transmission line network with nonlinear loads [11].

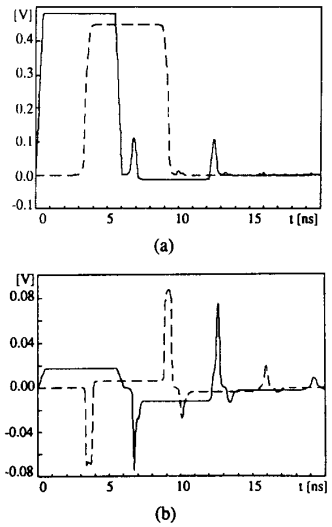

Fig. 19. Responses of the transmission line network of Fig. 18. (a) Voltages on active line. (b) Voltages on passive line.

The line transit time of the even and the odd mode is 3.376 ns and 3.290 ns, respectively. The simulation time step was chosen to be 40 ps. The simulation results are shown in Fig. 19(a) and (b). Fig. 19(a) shows the voltages at beginning and end of the driven line, and Fig. 19(b) shows the forward and backward crosstalk on the passive line. The full (dashed-) lines show the voltage at the left (right) side of the network. The results are in good agreement with [11].

VI. Conclusion

A new equivalent circuit model is presented for transient analysis of uniform and nonuniform interconnection structures with arbitrary linear and nonlinear loads. The extended scattering matrix description guarantees short impulse responses and a fast simulation algorithm with relatively small memory requirements. At each point in time, all ports of the interconnection network are decoupled and represented by an extended Thevenin equivalent. This equivalent circuit representation can be implemented in existing simulation programs, and can be used with arbitrary loading networks.

Acknowledgment

The authors wish to thank the editor and the anonymous referees for their helpful comments. The authors gratefully acknowledge the contribution of Peter Degraeuwe and Frank Olyslager in the preparation of the numerical examples.

References

[1] W. R. Klopfenstein, "A transmission line taper of improved design," *Proc. IRE*, pp. 31–35, June 1956.
[2] C. P. Womack, "The use of exponential transmission lines in microwave components," *IRE Trans. Microwave Theory Tech.*, pp. 124–132, Mar. 1962.
[3] W. M. Kaufman and S. J. Garret, "Tapered distributed filters," *IRE Trans. Circuit Theory*, pp. 329–336, Dec. 1962.
[4] S. Yamamoto, T. Azakami, and K. Itakura, "Coupled nonuniform transmission line and its applications," *IEEE Trans. Microwave Theory Tech.*, vol. 15, pp. 220–231, Apr. 1967.
[5] I. Endo, Y. Nemoto, and R. Sato, "Impedance transformation and matching for lumped complex load with nonuniform transmission line," *IEEE Trans. Microwave Theory Tech.*, vol. 33, pp. 2–8, Jan. 1985.
[6] ——, "Design of transformerless quasi-broadband matching networks for lumped complex loads using nonuniform transmission lines," *IEEE Trans. Microwave Theory Tech.*, vol. 36, pp. 629–634, Apr. 1988.
[7] G. M. Gladwell, S. R. Dods, and S. K. Chaudhuri, "Nonuniform transmission-line synthesis using inverse eigenvalue analysis," *IEEE Trans. Circuits Syst.*, vol. 35, pp. 659–666, June 1988.
[8] L. A. Hayden and V. K. Tripathi, "Nonuniformly coupled microstrip transversal filter for analog signal processing," *IEEE Trans. Microwave Theory Tech.*, vol. 39, pp. 47–53, Jan. 1991.
[9] K. J. Sterns, "Shaping fast rise-time pulses with tapered transmission lines," *IEEE Trans. Instrum. Meas.*, vol. 21, Aug. 1972.
[10] S. C. Burkhart and R. B. Wilcox, "Arbitrary pulse shape synthesis via nonuniform transmission lines," *IEEE Trans. Microwave Theory Tech.*, vol. 38, pp. 1514–1518, Oct. 1990.
[11] A. R. Djordjevic, T. K. Sarkar, and R. F. Harrington, "Analysis of lossy transmission lines with arbitrary nonlinear terminal networks," *IEEE Trans. Microwave Theory Tech.*, vol. 34, pp. 660–666, June 1986.
[12] T. Dhaene and D. De Zutter, "Selection of lumped elements models for coupled lossy transmission lines," *IEEE Trans. Computer-Aided Design*, vol. 11, pp. 805–815, July 1992.
[13] ——, "Extended scattering matrix approach for transient analysis of coupled dispersive lossy transmission lines with arbitrary loads," *Electromagnetics*, to be published 1993.
[14] E. R. Schatz and E. M. Williams, "Pulse transients in exponential transmission lines," *Proc. IRE*, pp. 1208–1212, Oct. 1950.
[15] J. L. Hill and D. Mathews, "Transient analysis of systems with exponential transmission lines," *IEEE Trans. Microwave Theory Tech.*, vol. 25, pp. 777–783, Sept. 1977.
[16] K. Kobayashi, Y. Nemoto, and R. Sato, "Equivalent circuits of binomial form nonuniform coupled transmission lines," *IEEE Trans. Microwave Theory Tech.*, vol. 29, pp. 817–824, Aug. 1981.
[17] I. Endo, Y. Nemoto, and R. Sato, "Equivalent representations of lossy nonuniform transmission lines," *IEEE Trans. Microwave Theory Tech.*, vol. 31, pp. 457–462, June 1983.
[18] H. Curtins and A. V. Shah, "Step response of lossless nonuniform transmission line with power-law characteristic impedance function," *IEEE Trans. Microwave Theory Tech.*, vol. 33, pp. 1210–1212, Nov. 1985.
[19] C.-W. Hsue, "Time-domain scattering parameters of an exponential transmission line," *IEEE Trans. Microwave Theory Tech.*, vol. 39, pp. 1891–1895, Nov. 1991.
[20] P. Pramanick and R. R. Mansour, "Dispersion characteristics of square pulse with finite rise time in single, tapered and coupled microstrip lines," *IEEE Trans. Microwave Theory Tech.*, vol. 39, pp. 2117–2122, Dec. 1991.
[21] Y. C. Yang, J. A. Kong, and Q. Gu, "Time-domain perturbational analysis of nonuniformly coupled transmission lines," *IEEE Trans. Microwave Theory Tech.*, vol. 33, pp. 1120–1130, Nov. 1985.
[22] Q. Gu, J. A. Kong, and Y. C. Yang, "Time-domain analysis of nonuniformly coupled line systems," *J. El. Waves Appl.*, vol. 1, pp. 109–132, 1987.
[23] O. A. Palusinski and A. Lee, "Analysis of transients in nonuniform and uniform multiconductor transmission lines," *IEEE Trans. Microwave Theory Tech.*, vol. 37, pp. 127–138, Jan. 1989.

[24] N. Orhanovic and V. K. Tripathi, "Time domain simulation of uniform and nonuniform multiconductor lossy lines by the method of characteristics," in *Proc. IEEE MTT-S: Int. Microwave Symp.*, pp. 1191–1194, 1990.
[25] M. A. Mehalic and R. Mittra, "Investigation of tapered multiple microstrip lines for VLSI circuits," *IEEE Trans. Microwave Theory Tech.*, vol. 38, pp. 1559–1567, Nov. 1990.
[26] D. Winkelstein, M. B. Steer, and R. Pomerleau, "Simulation of arbitrary transmission line networks with nonlinear terminations," *IEEE Trans. Circuits Syst.*, vol. 38, pp. 418–422, Apr. 1991.
[27] ——, "Corrections to 'Simulation of arbitrary transmission line networks with nonlinear terminations'," *IEEE Trans. Circuits Syst.*, vol. 38, p. 1238, Oct. 1991.
[28] F.-Y. Chang, "Waveform relaxation analysis of nonuniform lossy transmission lines characterized with frequency-dependent parameters," *IEEE Trans. Circuits Syst.*, vol. 38, pp. 1484–1500, Dec. 1991.
[29] Q. Gu, D. M. Sheen, and S. M. Ali, "Analysis of transients in frequency-dependent interconnections and planar circuits with nonlinear loads," *Proc. Inst. Elec. Eng., H*, vol. 139, pp. 38–44, Feb. 1992.
[30] J.-F. Mao and Z.-F. Li, "Analysis of the time response of multiconductor transmission lines with frequency-dependent losses by the method of convolution-characteristics," *IEEE Trans. Microwave Theory Tech.*, vol. 40, pp. 637–644, Apr. 1992.
[31] ——, "Analysis of the time response of nonuniform multiconductor transmission lines with a method of equivalent cascaded network chain," *IEEE Trans. Microwave Theory Tech.*, vol. 40, pp. 948–954, May 1992.
[32] J. E. Schutt-Aine, "Transient analysis of nonuniform transmission lines," *IEEE Trans. Circuits Syst.–I*, vol. 39, pp. 378–385, May 1992.
[33] Hewlett Packard, "*S*-Parameter Design," Application note 154.
[34] HP 85150B Microwave Design System (HP MDS).
[35] T. Dhaene and D. De Zutter, "Extended Thevenin models for transient analysis of nonuniform dispersive lossy multiconductor transmission lines," in *Proc. IEEE Int. Symp. Circuits and Systems* (ISCAS'92), vol. 4, pp. 1772–1775, May 1992.
[36] T. Dhaene, L. Martens, P. Degraeuwe, and D. De Zutter, "Improved time-domain characterization of high-speed interconnection structures," in *Proc. IEEE Topical Meeting on Electrical Performance of Electronic Packaging*, pp. 142–144, Apr. 1992.
[37] B. J. Cooke, J. L. Prince, and A. C. Cangellaris, "*S*-parameter analysis of multiconductor, integrated circuit interconnect systems," *IEEE Trans. Computer Aided Design*, vol. 11, pp. 353–360, Mar. 1992.
[38] F. J. Harris, "On the use of windows for harmonic analysis with the discrete Fourier transform," *Proc. IEEE*, vol. 66, pp. 51–83, Jan. 1978.
[39] C.-W. Ho, A. E. Ruehli, and P. A. Brennan, "The modified nodal approach to network analysis," *IEEE Trans. Circuits Syst.*, vol. 22, pp. 504–509, June 1975.
[40] S. Criel, "Signal propagation on multiconductor transmission lines," (in Dutch) M. Sc. thesis, Univ. Ghent—LEA, May 1991.
[41] L. Martens, P. Degraeuwe, D. De Zutter, R. Bargain, and D. Morlion, "Accurate characterization of a high-speed high-density multichip connector," in *Proc. Topical Meeting on Electrical Performance of Electronic Packaging*, pp. 131–133, Apr. 1992.
[42] T. Dhaene and D. De Zutter, "CAD-oriented general circuit description of uniform coupled lossy dispersive waveguide structures," in *Proc. IEEE Microwave Theory and Techniques—Special Issue on Process-Oriented Microwave CAD and Modeling*, vol. 40, pp. 1545–1554, July 1992.
[43] F. Olyslager, D. De Zutter, and K. Blomme, "Rigorous analysis of the propagation characteristics of general lossless and lossy multiconductor transmission lines in multilayered media," *IEEE Trans. Microwave Theory Tech*, to be published.

Tom Dhaene received the degree in electrical engineering from the University of Ghent, Belgium, in 1989.

He is currently working towards the Ph.D. degree in electrical engineering at the Laboratory of Electromagnetism and Acoustics (LEA) of the same university. His research focuses on all aspects of circuit modeling and circuit simulation of high-frequency and high-speed interconnections.

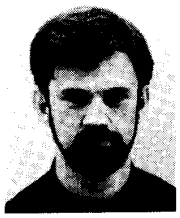

Luc Martens received the degree in electrical engineering from the University of Ghent in July 1986, and the Ph.D. degree in 1990.

From September 1986 to December 1990 he was a research assistant in the Laboratory of Electromagnetism and Acoustics (LEA) at the same university. During this period, his scientific work was focussed on the physical aspects of hyperthermic cancer therapy. His research work dealt with electromagnetic and thermal modelling and with the development of measurement systems for that application, which led to his Ph.D. degree. Since January 1991, he is at the same laboratory for the research in hyperthermia and biological effects of electromagnetic radiation, but his main research activities are in the field of high-frequency measurements.

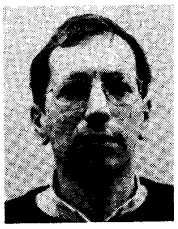

Daniël De Zutter received a degree in electrical engineering from the University of Ghent in July 1976.

In October 1981 he obtained a Ph. D. degree there and in the spring of 1984 he completed a thesis leading to a degree equivalent to the French Aggrégation or the German Habilitation. From September 1976 to September 1984 he was a research and teaching assistant in the Laboratory of Electromagnetism and Acoustics (LEA) at the same university. He is now a Professor at Ghent University and Research Director at the National Science Foundation of Belgium. Most of his earlier scientific work dealt with the electrodynamics of moving media, with emphasis on the Doppler effect and Lorentz forces. His research now focuses on all aspects of circuit and electromagnetic modeling of high-speed and high-frequency interconnections.

In 1990 Dr. De Zutter was elected as a member of the Electromagnetics Society.